JOURNAL OF MATERIALS SCIENCE 28 (1993) 3557–3563

Texture study of two molybdenum shaped charge liners by neutron diffraction

C. S. CHOI
Energetics and Warheads Division, ARDEC, Picatinny Arsenal, NJ 07806, and Reactor Radiation Division, NIST, Gaithersburg, MD 20899, USA

H. J. PRASK
Reactor Radiation Division, MSEL, NIST, Gaithersburg, MD 20899, USA

J. OROSZ, E. L. BAKER
Energetics and Warheads Division, ARDEC, Picatinny Arsenal, NJ 07806, USA

The textures of two different conical shaped liners, fabricated by the same forging processes from arc-cast and powder-sintered ingots, were investigated by using neutron-diffraction measurements and three-dimensional orientation-distribution-function (ODF) analysis. The major textures of both liners could be described by the (1 1 1)⟨*u v w*⟩ and (1 0 0)⟨*u v w*⟩ type. The two liners had essentially identical texture at the 8 cm position (measured from the base of the cone) with strong sheet-type texture components, i.e. (1 1 1)⟨$\bar{1}$ 0 1⟩, (1 1 1)⟨$\bar{1}$ 1 0⟩ and (1 0 0)⟨0 1 1⟩. However, the dominant textures at the 3 cm positions were ⟨1 1 1⟩ and ⟨1 0 0⟩ fibre textures with the fibre axes oriented parallel to the normal direction in both liners. A strong cube texture was observed at the 3 cm position of the arc-cast liner but it was not observed for the powder-sintered liner. The arc-cast liner had a generally higher degree of texture than the powder-sintered liner.

1. Introduction

It is well known that the textures in polycrystalline metals play a significant role in the plasticity and other physical properties of the materials. However, application of texture information to the improvement of material properties or to the design of fabrication processes is not a common practice yet, partly because of the difficulty of obtaining quantitative three-dimensional orientation distribution functions (ODFs). Since the two pioneering works of Roe [1] and by Bunge [2], several new quantitative ODF analysis methods have been developed. Until a few years ago, the use of ODF analysis was limited by the complexity of the mathematical calculations involved. Very recently, a comprehensive ODF analysis program package, called popLA, has been developed by Kallend *et al.* [3], it is designed to make modern ODF analysis methods available to the materials-science community.

The basic theory of the formation of armour-piercing metallic jets from conical shaped charge liners has been presented by Birkhoff *et al.* [4] and later by Pugh *et al.* [5], based on hydrodynamic theory, assuming that the liner metals can be treated as ideal fluids since the pressures and energies involved are so large. This theory assumes that the mechanical properties of the liner metals have a negligible effect on jet formation. However, there is considerable experimental evidence to suggest that the crystallographic texture of the liners plays an important role in jet formation and stability – as demonstrated by spin compensation by means of liner textures [6], and the stabilization of the jet by using the effect of the (1 1 1) texture of the liners [7]. Recently, researchers at the Naval Surface Warfare Center, White Oak, MD, USA (NSWC) have conducted a systematic study of the microstructures of tantalum liners [8–10]. This study suggests that the textures of the liners are quite sensitively related to the performance of the munitions.

The present study is intended to determine the three-dimensional ODF of two molybdenum liners fabricated from different ingots, arc-cast ingots and ingots formed from metallurgically sintered powder. The pole-figure data were collected by a neutron-diffraction method. Since neutrons penetrate into the whole body of the samples, the resultant ODFs are representative of the entire thickness of the liner and not just the surface texture. The computer program popLA was used for the ODF analysis.

2. Sample preparation

Two different types of molybdenum cones (approximately 8 cm in base diameter, 11 cm in height and about 0.6 cm in thickness) were supplied by the Picatinny Arsenal. One type of cone was fabricated from a vacuum-arc-cast ingot, and the other from a metallurgically-sintered-powder ingot. Both cones were fabricated using the same forming processes, including stress-relief annealing. Two rectangular plate-like specimens were cut from each liner for the texture study, one from a distance of between 2.5 and 3.5 cm from the base of the cone (called the 3 cm position), and the

0022–2461

other from the section between 7. 5 and 8.5 cm (called the 8 cm position). The specimens from the 3 cm position were approximately $10 \times 12 \times 6\ mm^3$ for the arc-cast liner (labelled MoC3) and $9 \times 11 \times 6\ mm^3$ for the sintered liner (labelled MoS3), and those from the 8 cm position were approximately $5 \times 8 \times 6\ mm^3$ for both the arc-cast (labelled MoC8) and the sintered liner (labelled MoS8).

3. Experimental procedure

The samples were mounted on a diffractometer, the normal to the cone surface (ND) is defined as the north pole and the cone-apex direction (RD) is defined as the origin of the ϕ-angle of the sample orientation hemisphere (i.e. pole figure). The pole-figure data of the four reflections, (1 1 0), (2 0 0), (2 1 1) and (2 2 2) were measured over an entire orientation hemisphere with 0.125 nm neutrons at the NIST research reactor. The observed data were corrected for background radiation. Absorption corrections were applied for the two larger specimens, MoC3 and MoS3, by using the calculated linear absorption coefficient, $\mu = 0.045\ mm^{-1}$. The corrected diffraction intensities were converted to pole densities in units of multiples-of-the-random-distribution (m.r.d.), by normalizing to the intensities averaged over the entire orientation hemisphere.

3.1. Arc-cast liner

The ODFs of the sample at the 3 cm position (MoC3) were obtained by the WIMV method, using triclinic sample symmetry. The WIMV analysis converged to 0.8% in the RP error parameter, residual of pole densities as defined by Matthies *et al.* [11], after 25 iterations. The recalculated pole figures are compared with the corresponding experimental pole figures in Fig. 1. The agreement between the experimental and the recalculated pole figures is excellent. This is clear evidence that the ODF describes the true texture very well. The three-dimensional ODF, in the form of the sample-orientation distribution (SOD), defined with Kocks-type Euler angles, is projected on the constant ψ-plane in Fig. 2. There are two different pole-density tubes running parallel to the ψ-axis in the SOD map, namely a 1 1 1 tube and a 1 0 0 tube. This indicates that (1 1 1)[$u\,v\,w$] and (1 0 0)[$u\,v\,w$] are the two dominant textures in the sample. The pole-density distributions of (1 1 1)[$u\,v\,w$] and (1 0 0)[$u\,v\,w$] as a function of the ψ-angles were extracted from the three-dimensional ODF, by using a two-dimensional linear interpolation at each ψ-angle level. These two ψ-angular distributions are shown in Fig. 3. The Miller indices corresponding to the [$u\,v\,w$] at each ψ-angle were calculated from the orientation matrix. The (1 1 1)[$u\,v\,w$] distribution in Fig. 3b shows strong peaks at the ψ-angles corresponding to the three (1 1 1)$\langle\bar{1}\,1\,0\rangle$ type orientations (related by the three-fold symmetry). They were superimposed on the [1 1 1] fibre texture (the fibre-axis orientation perpendicular to the cone surface) which maintains a constant intensity over the entire ψ-angle range. The average orientation densities of the (1 1 1)$\langle\bar{1}\,1\,0\rangle$ orientations were about 9 m.r.d and those of the [1 1 1] fibre texture about 6 m.r.d. It is interesting to notice that the (1 1 1)$\langle\bar{1}\,0\,1\rangle$ type orientations have considerably weaker density than the (1 1 1)$\langle\bar{1}\,1\,0\rangle$ type orientation. Since the two crystal orientations are related by the mirror-symmetric equivalency in the cubic lattice, the difference in the two orientation densities is a manifestation of the asymmetric textures about the ND–RD plane of the

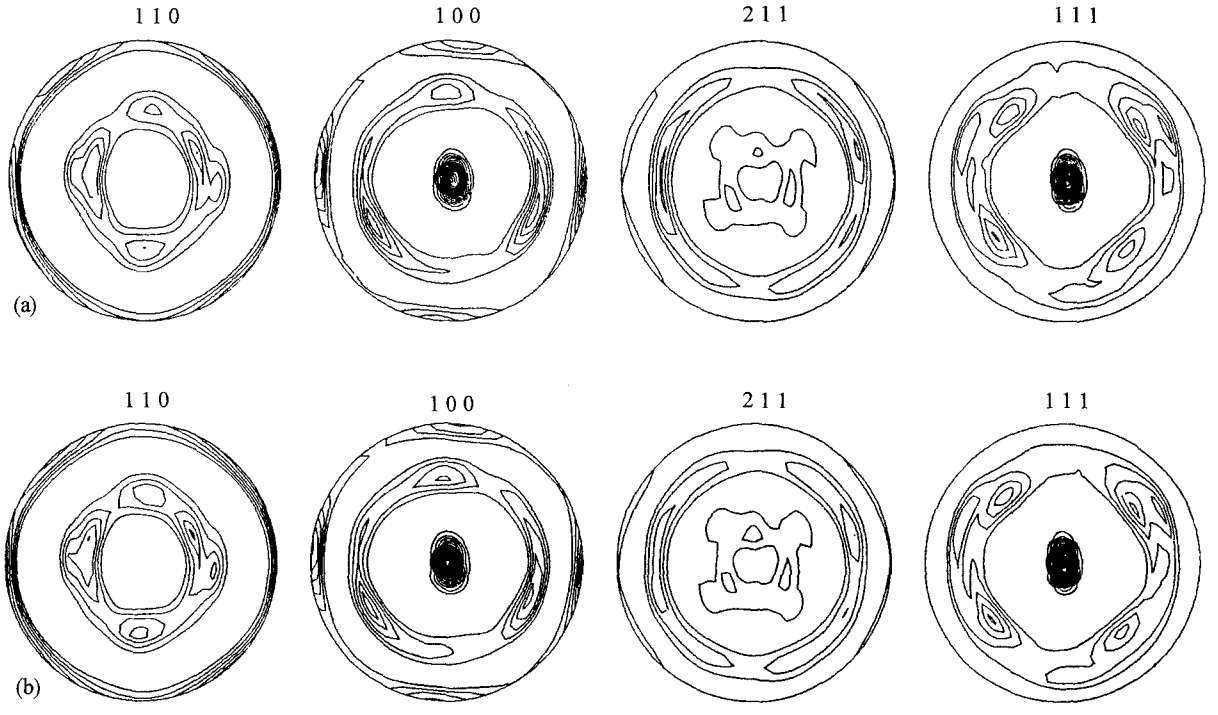

Figure 1 MoC3 sample: (a) experimental pole figures, and (b) the corresponding recalculated pole figures. Contour levels of 1 m.r.d. and higher are given at 0.5 m.r.d. intervals. The RD (direction toward the cone apex) is at the 3 o'clock position and the ND (direction normal to the cone surface) is at the centre of the pole figure.

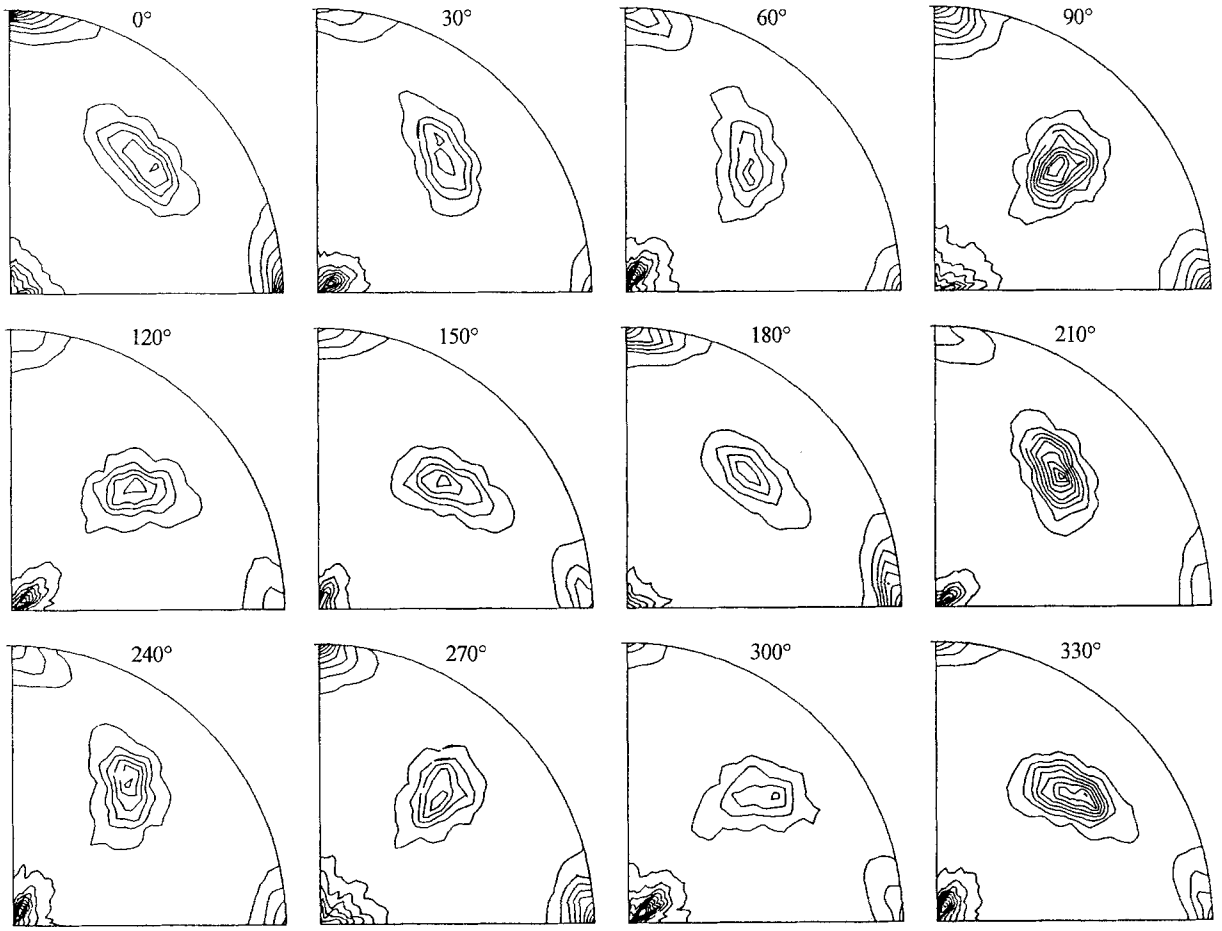

Figure 2 The SODs of MoC3, defined by Kocks-type Euler angles, are presented in the constant ψ-planes, for $\psi = 0$–$330°$ in 30° intervals. The [1 0 0] direction of the crystal co-ordinate system is at the right edge, [0 1 0] at the top, and [0 0 1] at the centre of the quadrants.

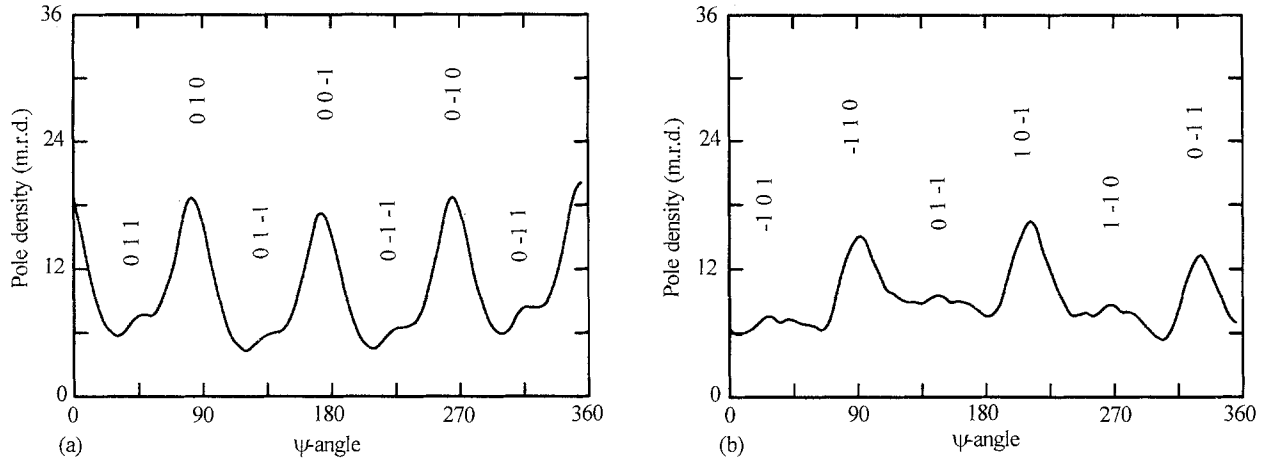

Figure 3 The orientation distributions of the MoC3 sample are presented as a function of the ψ-angles: (a) (1 0 0) [$u\,v\,w$], and (b) (1 1 1) [$u\,v\,w$]. The Miller indices of [$u\,v\,w$] corresponding to each peak orientation are included.

sample. This texture asymmetry can be seen clearly from the pole figures in Fig. 1, which are clearly asymmetric about the ND–RD planes (horizontal diameters). The (1 0 0)[$u\,v\,w$] distribution showed four strong peaks at ψ-angles corresponding to the (1 0 0) ⟨0 1 0⟩ orientations (commonly called cube texture), with average intensity of about 19 m.r.d. including the [1 0 0] fibre texture intensity. If the pole density of the [1 0 0] fibre intensity is estimated to be about 5 m.r.d., the net pole density of the (1 0 0)⟨0 1 0⟩ texture becomes about 14 m.r.d. The (1 0 0)⟨0 1 1⟩ type texture was also observed in the (1 0 0)[$u\,v\,w$] distribution although the intensities were quite weak. The texture components found for the MoC3 sample are compared with those of the other sample in Table I.

The ODF of the sample representing the 8 cm position (MoC8) was obtained similarly by the WIMV method using triclinic sample symmetry. The RP parameter was reduced to 1.6% after 25 iterations. Although only three pole figures (1 1 0), (1 0 0) and (2 1 1) were used for the WIMV analysis, the recalculated pole figures from the ODF show excellent

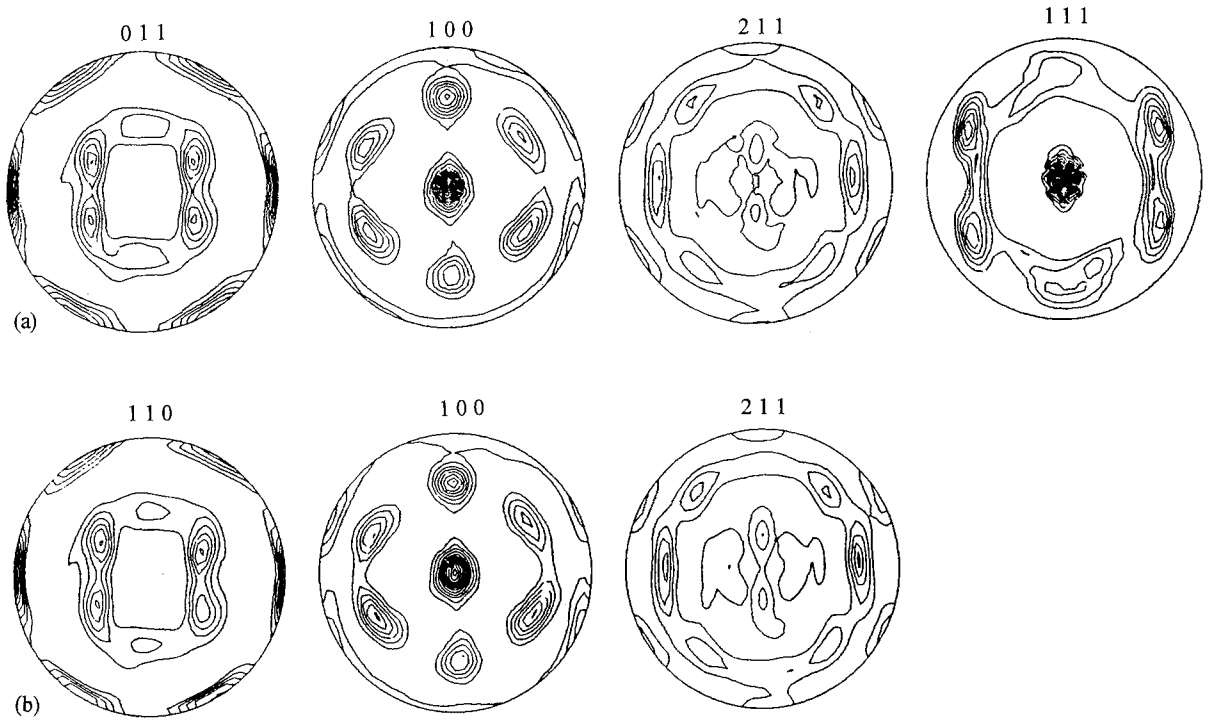

Figure 4 (a) the corresponding recalculated pole figures. Contour levels of 1 m.r.d. and higher are given in 0.5 m.r.d. steps, and (b) Experimental pole figures of the MoC8 sample.

TABLE I Major texture components of the two conical molybdenum liners, arc-cast (MoC type) and powder-sintered (MoS type). The [1 0 0] and [1 1 1] fibre axes in the table are oriented perpendicularly to the cone surface.

Specimen	Texture index	Texture	pole density (m.r.d)
MoC3	2.3	(1 1 1)⟨$\bar{1}$ 1 0⟩	9
		[1 1 1] fibre	6
		(1 0 0) ⟨0 1 0⟩	14
		(1 0 0) ⟨0 1 1⟩	2
		[1 0 0] fibre	5
MoC8	2.3	(1 1 1)⟨$\bar{1}$ 1 0⟩	19
		(1 1 1) ⟨$\bar{1}$ 0 1⟩	14
		(1 0 0) ⟨0 1 1⟩	12
		(1 1 2) ⟨$\bar{1}$ 1 0⟩	5
MoS3	2.1	(1 1 1)⟨$\bar{1}$ 2 $\bar{1}$⟩	3
		[1 1 1] fibre	7
		(1 0 0) ⟨0 1 1⟩	6
		[1 0 0] fibre	6
MoS8	2.0	(1 1 1)⟨$\bar{1}$ 0 1⟩	15
		(1 1 1) ⟨$\bar{1}$ 1 0⟩	10
		(1 0 0) ⟨0 1 1⟩	8
		(1 1 2) ⟨$\bar{1}$ 1 0⟩	5
		[1 0 0] fibre	4

agreement with the experimental pole figures, as in Fig. 4. The SOD of the MoC3 sample exhibited three major textures, (1 1 1)[$u v w$], (1 0 0)[$u v w$] and (1 1 2) ⟨$\bar{1}$ 1 0⟩. The (1 1 1)[$u v w$] orientation distributions, given in Fig. 5b, reveal well defined and strong (1 1 1) ⟨$\bar{1}$ 1 0⟩ and (1 1 1) ⟨$\bar{1}$ 0 1⟩ texture, and the (1 0 0) [$u v w$] distributions show broadly defined {1 0 0} ⟨0 1 1⟩ textures, ranging from {1 0 0}⟨0 1 3⟩ to {1 0 0} ⟨0 3 1⟩. There was no evidence of fibre textures in the MoC8 sample.

It is quite interesting to note that the texture of the arc-cast liner clearly changes with distance from the base. The cube texture {1 0 0}⟨0 1 0⟩, is the most dominant texture at the 3 cm position, is not a preferential orientation at the 8 cm position. However, the strong sheet-type textures which dominate at the 8 cm position, i.e. (1 1 1)⟨$\bar{1}$ 0 1⟩ and (1 0 0)⟨0 1 1⟩, are reduced almost to the level of the fibre texture at the 3 cm position, and the (1 1 1)⟨$\bar{1}$ 1 0⟩ peak is barely above the fibre level.

3.2. Powder-metallurgical liner

The ODF of the sample at the 3 cm position (MoS3) was also obtained by using WIMV analysis with triclinic sample symmetry. The RP error parameter was reduced to 1.2% after 20 iterations. The recalculated pole figures obtained from the ODF agreed well with the corresponding experimental pole figures, as shown in Fig. 6. The SOD showed two pronounced texture types, (1 1 1)⟨$u v w$⟩ and (1 0 0)⟨$u v w$⟩. These two orientation density distributions are presented in Fig. 7 revealing three major textures, i.e. (1 0 0)⟨0 1 1⟩, ⟨1 0 0⟩ fibre parallel to the ND, and ⟨1 1 1⟩ fibre parallel to the ND. In addition, there is evidence of a weak (1 1 1)⟨$\bar{1}$ 2 $\bar{1}$⟩ texture, as can be seen from the (1 1 1)⟨$u v w$⟩ distribution in Fig. 7.

It was noticed after the data collection that the sample representing the 8 cm position (MoS8) was mounted with the ND tilted more than 5° from the diffractometer ϕ-axis (the ND of the pole figure). The distortion of the pole figures due to this misorientation was corrected by tilting the ND axis of the sample co-ordinates. The ODF of the sample was also obtained by using WIMV analysis with triclinic sample symmetry. The RP parameter was reduced to 1.1%

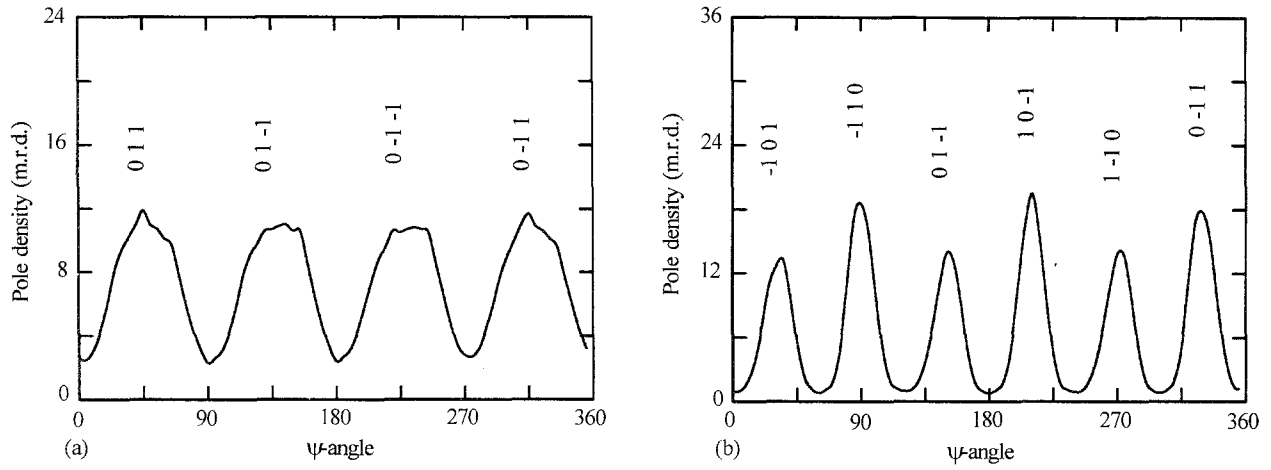

Figure 5 Orientation distributions of the MoC8 sample are presented as a function of the ψ-angles: (a) (1 0 0) [*u v w*], and (b) (1 1 1) [*u v w*]. The Miller indices of [*u v w*] corresponding to each peak orientation are given.

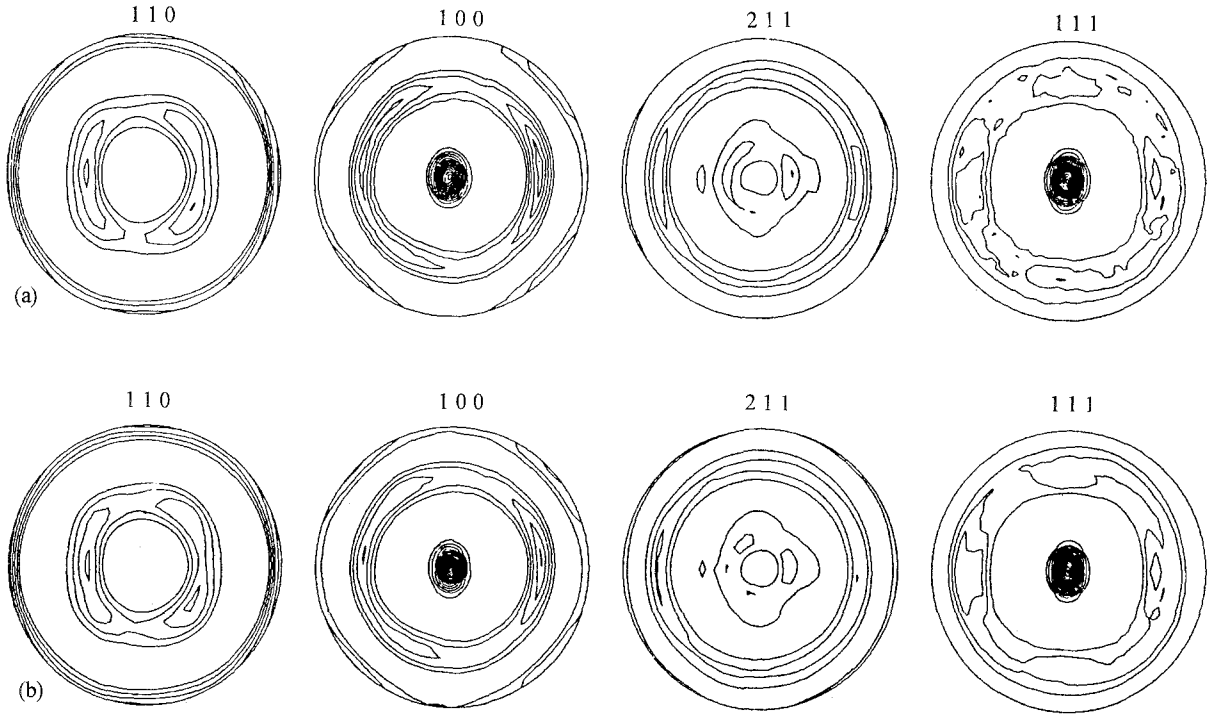

Figure 6 (a) the experimental pole figures of the MoS3 sample, and (b) the corresponding recalculated pole figures of the MoS3 sample. Contour levels of 1 m.r.d and higher are given in 0.5 m.r.d. steps.

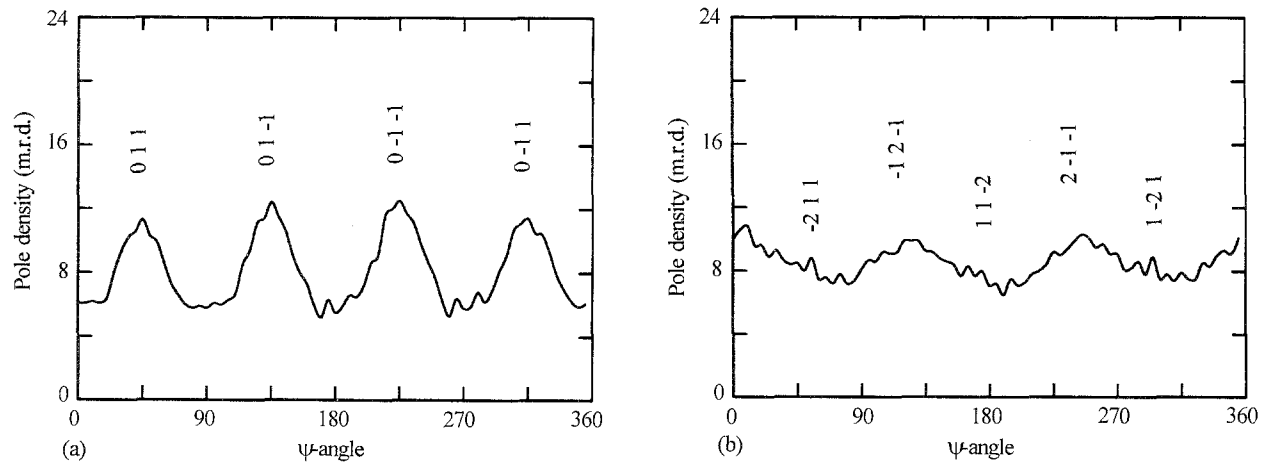

Figure 7 Orientation distributions of the MoS3 sample are presented as a function of the ψ-angles: (a) (1 0 0) [*u v w*], and (b) (1 1 1) [*u v w*]. The Miller indices of the [*u v w*] corresponding to each peak orientation are shown.

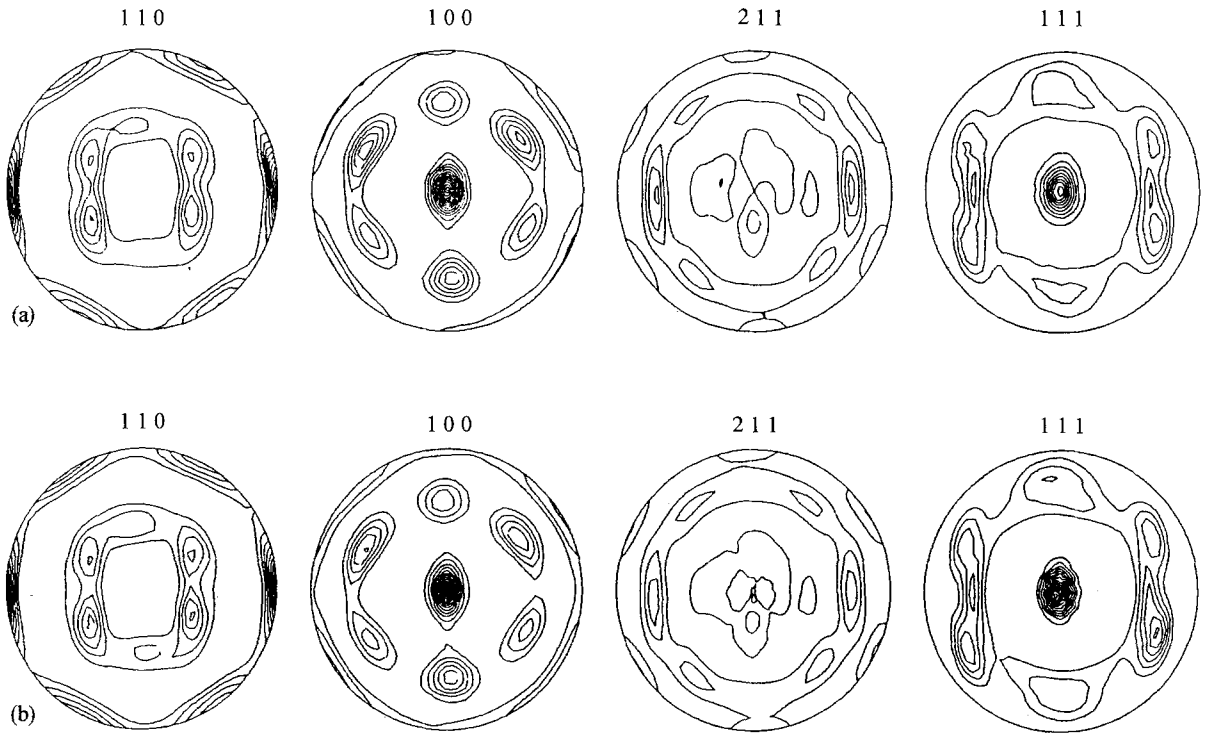

Figure 8 Pole figures of the MoS8 sample: (a) experimental and (b) corresponding recalculated pole figures. Contour levels of 1 m.r.d. and higher are given in 0.5 m.r.d. steps.

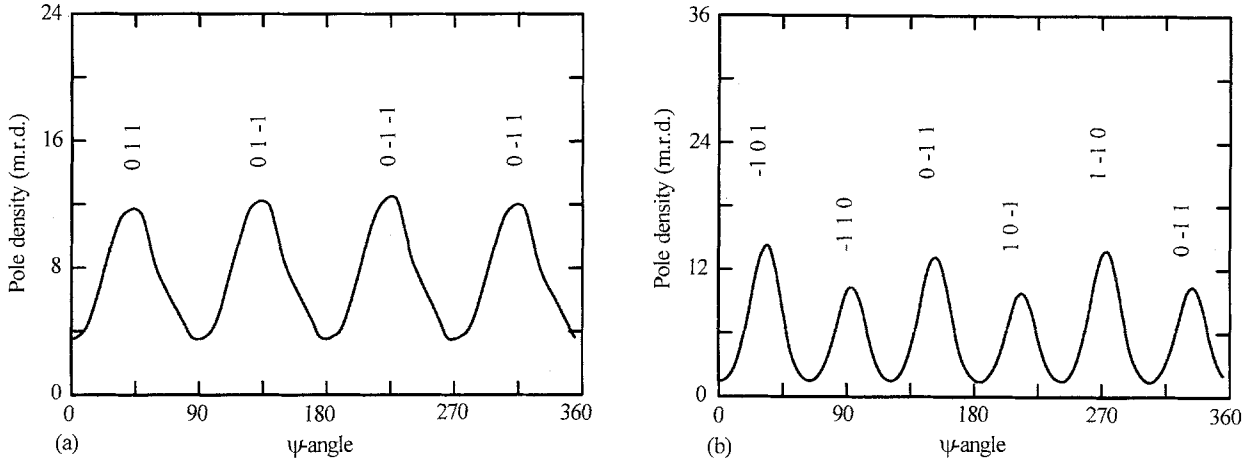

Figure 9 Orientation distributions of the MoS8 sample are presented as a function of the ψ-angles: (a) (1 0 0) [*u v w*], and (b) (1 1 1) [*u v w*]. The Miller indices of the [*u v w*] corresponding to each peak orientation are included.

after 20 iterations. The recalculated pole figures from the ODF agreed extremely well with the experimental pole figures, as compared in Fig. 8. The SOD exhibited two major texture types, (1 1 1)⟨*u v w*⟩ and (1 0 0) ⟨*u v w*⟩. The (1 1 1)⟨*u v w*⟩ distribution (Fig. 9b) revealed two sheet-type textures: (1 1 1)⟨$\bar{1}$ 0 1⟩ with an average intensity of 15 m.r.d and (1 1 1)⟨$\bar{1}$ 1 0⟩ with an average intensity of about 10 m.r.d. The (1 0 0)⟨*u v w*⟩ distribution exhibited a broad range of preferential orientation centred at {1 0 0}⟨0 1 1⟩ orientation with an average peak height of 12 m.r.d.

The texture of the powder-metallurgical liner is also dependent on the distance from the base of the cone. (1 1 1) ⟨$\bar{1}$ 0 1⟩ and (1 1 1) ⟨$\bar{1}$ 1 0⟩ are strong and pronounced preferential orientations at the 8 cm position, but they become a part of the [1 1 1] fibre texture at the 3 cm position. The [1 0 0] fibre textures are about twice as intense at the 3 cm position as at the 8 cm position.

4. Discussion

The two liners were fabricated by the same forging processes, including a post-annealing process, but from different ingots. The ingot of the MoC-type liner was obtained by the arc-cast method and that of the MoS-type by the powder-sintering method. Although the overall textures of the two liners are clearly different, they also contain some similar components. Particularly at the 8 cm position, both liners contain the same sheet-type texture components, i.e. (1 1 1) ⟨$\bar{1}$ 0 1⟩, (1 1 1) ⟨$\bar{1}$ 1 0⟩ and (1 0 0) ⟨0 1 1⟩, as shown in Table I. Consequently, the pole figures of the two samples (MoC8 and MoS8) are almost identical as can be seen

from Figs 4 and 8. Two sets of orientations, (1 1 1) $\langle \bar{1}\,0\,1 \rangle$ and (1 1 1)$\langle \bar{1}\,1\,0 \rangle$, are equivalent by the mirror symmetry in the cubic crystal, but show different intensity in both liners as can be seen from the (1 1 1) $[u\,v\,w]$ distributions in Figs 3, 5 and 9. Since the reference frames of the orientation space are the RD, TD and ND of the sample, the difference is attributable to the asymmetric texture about the ND–RD plane (the plane passing through the cone axis), but not to the crystal symmetry. At the 3 cm position, the sheet-types have changed mostly to the $\langle 1\,1\,1 \rangle$ and $\langle 1\,0\,0 \rangle$ fibre textures in both liners. The most significant difference between the two liners is the strong cube texture developed at the 3 cm position of the MoC-type liner. The MoC-type liner has a generally higher degree of texture than the MoS-type liner, as indicated by the texture indexes summarized in Table I.

In each liner, the texture at the 3 cm position is different from that at the 8 cm position. Since the final textures of the liners are the cumulative results of the two precursor textures, i.e. the annealing textures and the deformation textures, it is difficult to find the development process of the different textures. If the deformation textures of the liners had been measured before the annealing processes, the annealing effects could also be determined from the two studies. The variation of the textures by the positions within a liner is probably mainly attributable to the plastic deformations in the liner-forming stage.

The rolling textures and the annealing textures of several low-carbon steels have been studied extensively by Emren *et al.* [12]. The development of the recrystallization textures in the steel may merit comparison with the present results since the steel has the same crystal structure, body-centred cubic, as the molybdenum. In the unpinned steel materials (i.e. no C–Mn dipoles), Emren *et al.* found the formation of strong recrystallization textures, such as the $\langle 1\,1\,1 \rangle$ fibre texture with the fibre axis parallel to the ND and an incomplete $\langle 1\,1\,0 \rangle$ fibre with the fibre axis parallel to the RD, with the growth rate increased by increasing annealing temperature. This suggests that the pronounced (1 1 1) $\langle u\,v\,w \rangle$ textures formed in the two Mo liners are developed by annealing, at least in part.

References

1. R. J. ROE, *J. Appl. Phys.* **36** (1965) 2024.
2. H. J. BUNGE, *Z. Metallkde* **56** (1965) 872.
3. J. S. KALLEND, U. F. KOCKS, A. D. ROLLETT, and H. R. WENK, *Mater. Sci. Engng. A* **132** (1991) 1.
4. G. BIRKHOFF, E. M. MACDOUGALL and G. TATLOR, *J. Appl. Phys.* **19** (1948) 563.
5. E. M. PUGH, R. J. EICHELBERGER and N. ROSTOKER, *J. Appl. Phys.* **23** (1952) 532.
6. M. K. GAINER and C. M. GLASS, USA Ballistics Research Labortory (BRL) Report No. 1167, May (1962).
7. F. JAMET, in Proceedings of the Eighth International Symposium on Ballistics, Orlando, FL, USA, edited by W. G. Reinecke (AVCO Systems Division, Wilmington, MA, 1984), pp. v1–v6.
8. R. K. GARRETT Jr and J. B. CLARK, NSWC TR 88–30 (1988), Classified.
9. J. B. CLARK and R. K. GARRETT Jr, NSWC TR 88–104 (1989), Classified.
10. T. L. JUNGLING, R. K. GARRETT Jr, and J. B. CLARK, NSWC TR 88–106, (1989), Classified.
11. S. MATTHIES, H. R. WENK and G. W. VINEL, *J. Appl. Cryst.* **21** (1988) 285.
12. F. EMREN, U. VON SCHLIPPENBACH and K. LUCKE, *Acta Metall.* **34** (1986) 2105.

Received 8 April
and accepted 19 November 1992